ADVANCING EARTH AND SPACE SCIENCE

Water Resources Research

RESEARCH ARTICLE

10.1029/2020WR028852

Special Section:
Floodplains as Complex Adaptive Systems

Sediment Transport Potential in a Hydraulically Connected River and Floodplain-Channel System

Sumaiya Sumaiya[1], Jonathan A. Czuba[1], John T. Schubert[1,2], Scott R. David[3], Graham H. Johnston[4], and Douglas A. Edmonds[5]

[1]Department of Biological Systems Engineering, Virginia Tech, Blacksburg, VA, USA, [2]Now at Wetland Studies and Solutions, Inc., Roanoke, VA, USA, [3]Department of Watershed Sciences, Utah State University, Logan, UT, USA, [4]ExxonMobil, Spring, TX, USA, [5]Department of Earth and Atmospheric Sciences, Indiana University, Bloomington, IN, USA

Key Points:

- We investigate the potential of various sizes of sediment to move over a complex topographic floodplain surface at different flows.
- We compute an effective sediment size moved in suspension and as bedload by integrating the largest sediment size moved for all flows.
- We compare our effective sediment size with field data and conclude unvegetated floodplain channels are on a net erosional trajectory.

Correspondence to:
J. A. Czuba,
jczuba@vt.edu

Citation:
Sumaiya, S., Czuba, J. A., Schubert, J. T., David, S. R., Johnston, G. H., & Edmonds, D. A. (2021). Sediment transport potential in a hydraulically connected river and floodplain-channel system. *Water Resources Research*, *57*, e2020WR028852. https://doi.org/10.1029/2020WR028852

Received 15 SEP 2020
Accepted 18 APR 2021

Abstract

Meandering river floodplains often contain intermittently flooded complex channel networks. Many questions remain as to the pervasiveness, function, and evolution of these floodplain channels. In this present work, we analyzed size-specific sediment transport potential and assessed whether the channelized floodplain of the meandering East Fork White River near Seymour, Indiana is on a net erosional or depositional trajectory. We applied a two-dimensional hydrodynamic model and used simulated model results to estimate the largest sediment size that can be moved in suspension and as bedload at various flows for grain size classes between 4 μm and 64 mm. We developed a probabilistic method that integrates the largest sediment size that can be moved at various flows to compute an effective grain size, which we compared to measured field data. Results show that the river is capable of supplying sand to the floodplain and these floodplain channels can transport sand in suspension and gravel as bedload. This suggests that sediment supplied from the river could be transported as bedload in floodplain channels. These floodplain channels are supply limited under the current hydrologic regime and the grain size distribution of the bed surface is set by the flow conditions; thus, these floodplain channels are net erosional. Finally, our proposed method of probabilistically integrating the largest sediment size that can be moved at various flows can be used to predict the upper end of the grain size distribution in suspension and in bed material, which is applicable to floodplains as well as coastal areas.

1. Introduction

Floodplains are intermittently flooded complex geomorphic features with positive and negative relief (Lewin & Ashworth, 2014). Negative relief consists of meso- and macro-scale elements that include accessory through-channels, tributary channels, channel margin slackwater zones, bar-shelter backwaters, contiguous channel remnants, tie channels, internal drainage channel networks, and large-scale flood basins occluded by channel-belt aggradation (Lewin & Ashworth, 2014). This negative relief is present on both braided (Kleinhans & Berg, 2011; Limaye, 2017; Reinfelds & Nanson, 1993; Schuurman et al., 2013) and meandering (David et al., 2017; Lewin et al., 2017; Park & Latrubesse, 2017; Trigg et al., 2012) river floodplains. At least for meandering river floodplains, high-resolution topographic data reveal that negative relief is often organized into a floodplain-channel network (David et al., 2017; Lewin & Ashworth, 2014). These networks create well-connected river-floodplain systems, and examples include the Amazon River in Brazil (Mertes et al., 1996; Rudorff et al., 2014; Trigg et al., 2012), Medway River in southern Ontario (Thayer & Ashmore, 2016), Ogeechee River in Georgia (Benke et al., 2000), Congaree River in South Carolina (Kupfer et al., 2015; Xu et al., 2020), Copper Creek in Australia (Fagan & Nanson, 2004), Kolymar River in Russia (Lewin & Ashworth, 2014), Sava River in Slovenia (Rak et al., 2016), and White River in Indiana (Czuba et al., 2019; David et al., 2017).

The origin of well-connected river-floodplain systems is not entirely, but certainly due to overbank processes, which contribute to a richness of floodplain topographic forms, including floodplain channels of different sizes and shapes. The pathways through which floodwaters first inundate the floodplain can be focused through breaches, crevasses, and chutes which can actively erode the floodplain proximally and terminate into fan or lobe shaped crevasse splay deposits distally (Allen, 1965; Bristow et al., 1999; Brown, 1996; Lewin et al., 2017; O'Brien & Wells, 1986; Zwoliński, 1992). Floodplain channels are main conduits through which water and sediment are exchanged between a river and its floodplain (Czuba et al., 2019). During an overbank flood, at least suspended sediment from a river can be transported to the floodplain through these pathways and become deposited or resuspended, resulting in floodplain erosion/deposition depending on the flow conditions and supplied sediment (Zwoliński, 1992). Overall, a combination of overbank transport processes driven by water or wind, including turbulent diffusion and advection, can transport sediment in suspension and as bedload, leading to erosion and deposition and the formation of complex floodplain deposits and associated topography (Allen, 1965; Nanson, 1986; Phillips, 2011; Pizzuto et al., 2008). Floodplain surfaces built by periodic erosion and deposition consist of a range of grain sizes and typically fine with increasing distance from the main channel (Marriott, 1992; Nanson & Croke, 1992; Nicholas & Walling, 1996), however, floodplain topography can complicate this general pattern (Moody et al., 1999; Pizzuto et al., 2008).

Many floodplains described in the literature are formed from sediment deposited through lateral point-bar accretion of sand and/or gravel and vertical overbank deposition of finer sand, silt, and clay (Brown, 1996; Jackson, 1976; Lauer & Parker, 2008; Nanson, 1980; Nanson & Croke, 1992; Nunnally, 1967; Wolman & Leopold, 1957). These types of floodplains are classified as Type B3: Meandering river, lateral-migration floodplains (Nanson & Croke, 1992). Lateral point-bar accretion occurs where coarse bed-material sediment progressively deposits on the point bar along the inner bank of a meander bed due to secondary flow circulation within the river (e.g., Dietrich, 1987). Vertical overbank deposition occurs when floods deposit fine-grained suspended sediment on inundated areas adjacent to the channel. Additionally, levee crevasses deposit sandy splays on floodplains and abandoned oxbow lakes progressively fill with fine-grained material (e.g., Brown, 1996). This process of overbank flow and fine-grained sediment deposition on the floodplain is a necessary condition for sustained dynamic meandering in laboratory experiments (Van Dijk et al., 2013).

Yet despite our understanding of the feedbacks between overbank and in-channel processes, in the context of mathematical modeling, the floodplain has often been characterized as a flat feature adjacent to a river channel (at most with a further conceptualization of an associated levee, point bar, and/or sloping floodplain). The conceptualization of a featureless floodplain arises for reasons of data resolution and the need to simplify model geometry. This simple conceptualization appears in geomorphology (James, 1985; Lauer & Parker, 2008; Lauer & Willenbring, 2010; Nicholas et al., 2006; Pizzuto, 1987; Viparelli et al., 2013) and hydraulic engineering (see review by Knight & Shiono, 1996; Sturm, 2001). As a result, the full complexity of sediment transport dynamics on floodplains cannot be simulated using these simple models. Early attempts had been made at two-dimensional (2D) and three-dimensional modeling of flow and sedimentation patterns over floodplains with variable topography (Bates et al., 1996; Middelkoop & Perk, 1998; Nicholas & McLelland, 2004; Nicholas & Mitchell, 2003; Nicholas & Walling, 1997, 1998). However, at the time, these simulations had been limited by data resolution. High resolution topographic data reveal the complex nature of floodplains (David et al., 2017) and provide the opportunity to study surface processes on floodplains in more detail.

The purpose of this study is to investigate the potential of various sizes of sediment to move over a low-gradient, complex topographic floodplain surface at different flows. We focused our analysis on the same reach of the unconfined, meandering East Fork White River, Indiana, as described by Czuba et al. (2019). We first refined the 2-D HEC-RAS model of Czuba et al. (2019) and verified that the changes we made still agreed with the model calibration and validation data. We ran the model at 21 flows to simulate depth, velocity, and shear stress. We then used these simulated hydraulic data to estimate the largest sediment size that can be moved in suspension or as bedload spatially across the river-floodplain at various flows. By probabilistically integrating (based on flow recurrence) the largest sediment size that can be moved for all flows, we were able to compute an effective sediment size moved in suspension and as bedload. Finally, we compared our estimated effective sediment sizes with field data and used these estimates to assess whether this floodplain, and the floodplain channels specifically, are on a net erosional or depositional trajectory.

2. Study Area

The East Fork White River (EFWR) near Seymour, Indiana (Figures 1a and 1b) meanders through an agricultural floodplain with distinctive floodplain channels (Czuba et al., 2019; David et al., 2017). These floodplain channels are subtle, low-relief features that are difficult to differentiate in the field from general undulating topography. Historically, much of the White River basin (~29,400 km^2 drainage area) was

10.1029/2020WR028852

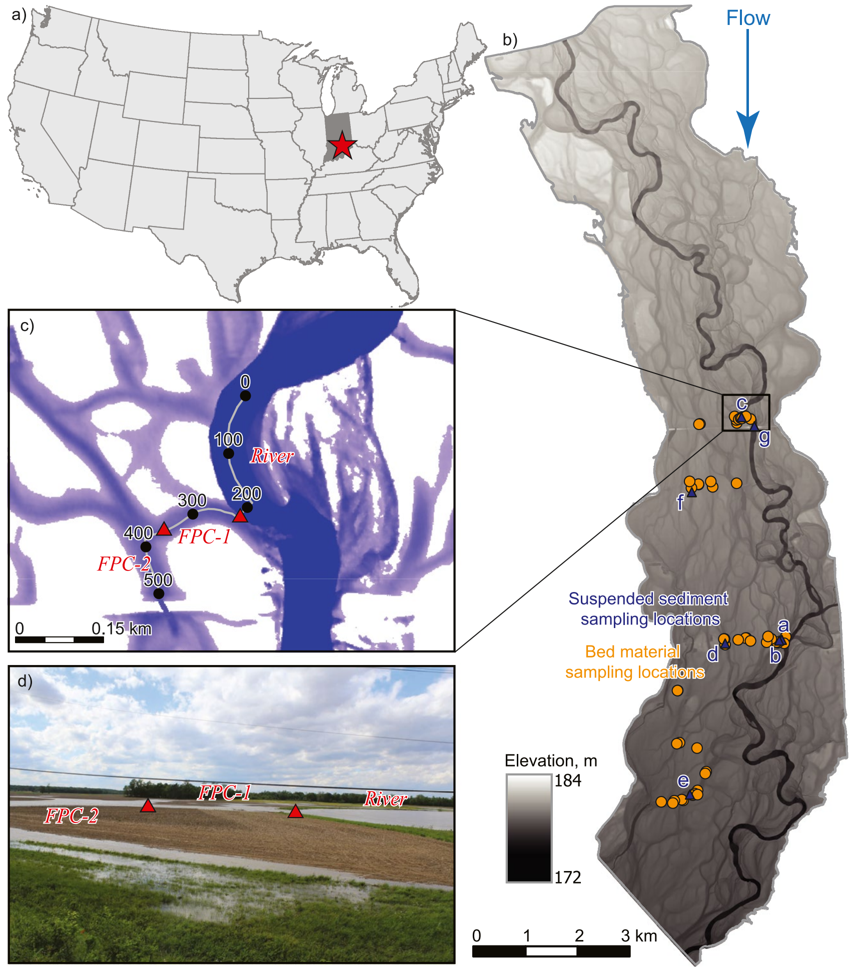

Figure 1. Study area of the East Fork White River (EFWR) near Seymour, Indiana (39° 5′ 11″ N, 85° 51′ 42″ W). (a) Red star represents the location of the EFWR in Indiana, USA. (b) Elevation of the river-floodplain system within an area of interest (AOI) prepared from the lidar data collected on March 23, 2011. Orange circles represent bed material sampling locations (47 total) and blue triangles represent suspended sediment sampling locations (8 total, labeled a-g; 1 not shown, labeled "h," located farther downstream). Black rectangular box indicates the highlighted flowpath location within the AOI. (c) Highlighted 500-m long flowpath with stationing (black circles) starting at 0 farthest upstream in the river. Red triangles represent the break points among the river and floodplain channels (FPC-1 and FPC-2). Blue area shows simulated inundated extent with darker blues corresponding to deeper depths; 454 m^3/s. (d) Picture of the flowpath taken on May 2, 2017 that corresponds to the simulated flood extent in (c).

forested, had been cleared during the 1800s, and is currently 56% agriculture, 30% forested, and 11% urban (Crawford et al., 1996; Homer et al., 2015).

Previous work in Indiana has taken advantage of state-wide, high-resolution (1.5 m) lidar data to learn that roughly 40% (by area) of floodplains throughout Indiana have floodplain channels (David et al., 2017). These floodplain channels are present most readily in wide, agricultural floodplains where the adjacent river has high migration rates (David et al., 2017). Additionally, these floodplain channels are a combination of old oxbows and likely more recent channels formed by upstream migrating headcuts connecting many floodplain lows, such as old oxbows and other topographic depressions, into an interconnected floodplain channel network (David et al., 2017, 2019). Of all the floodplains in Indiana investigated by David et al. (2017), the reach along the EFWR near Seymour had one of the most extensive floodplain channel networks without other factors appearing to influence its pattern, such as strong lateral floodplain slope, major backwater, or anthropogenic structures. In this reach specifically, these floodplain channels are inundated roughly 19 days per year, well before most river channel banks are overtopped (Czuba et al., 2019).

10.1029/2020WR028852

Our study focuses on a reach of the EFWR, which we call our area of interest (AOI, Figure 1b), that includes 24.4 km of the meandering river, measures 14.3 km along the floodplain valley centerline, and has a drainage area at its downstream end of roughly 6,000 km^2. The only major tributary that enters the study reach is Sand Creek, with a drainage area of 670 km^2. The slope of the river is roughly 3.2×10^{-4} m/m and the down-valley slope along the floodplain is roughly 5.5×10^{-4} m/m. The river channel here is roughly 90 m wide at the top of its banks with a 2.7 km wide floodplain (Figure 1b). Within the AOI in Figure 1b, the land cover is 76% agriculture (predominantly corn and soybean), 13% forested, 7% open water, and 3% urban (Homer et al., 2015).

For clarity in explaining the results that build from our methodology, we further focus on an ∼500-m long, river-to-floodplain flowpath (Figure 1c). Along this flowpath, stationing 0–216 m is within the river channel, stationing 216 m marks the river-floodplain boundary, and stationing 216–477 m is within the floodplain. Along this flowpath within the floodplain, there are two distinct floodplain channels: the floodplain channel at stationing 216–387 m connects the river to the floodplain channel network and flows perpendicular to the down-valley direction and the floodplain channel at stationing 387–477 m is a major segment of the floodplain channel network that conveys water that has largely entered the floodplain from farther upstream and flows parallel to the down-valley direction. This specific flowpath was selected because it is a location we were able to easily and safely return to during high flow because of nearby road access to collect various field data. The image (Figure 1d) of the flowpath (in Figure 1c) was taken during data collection on May 2, 2017. Prior to data collection, on April 30, 2017, the flow at a nearby USGS gage (03365500 East Fork White River at Seymour, Indiana; approximately 5.7 km along the channel centerline downstream from the AOI) peaked at 481 m^3/s. The flow then receded to 334 m^3/s on May 1, 2017 and 307 m^3/s on May 2. A corresponding model simulation at 454 m^3/s (simulated depth in blue, Figure 1c), which best matches the water-surface elevations measured in the floodplain (see Czuba et al., 2019 for discussion), shows the same amount floodplain inundation for comparison (Figure 1d).

3. Methods

3.1. Model Development, Calibration, Validation, and Simulations

We refined the 2-D HEC-RAS model (using version 5.0.5) for the EFWR of Czuba et al. (2019) in order to ensure the most accurate estimates of velocity and shear stress in floodplain channels. The full details describing the underlying data used to generate the terrain surface from 1.5-m lidar topography and surveyed river bathymetry, and data used in model calibration and validation can be found in Czuba et al. (2019). Here we only focus on the details we have changed in the model.

We refined the computational grid by adding additional breaklines with a nominal cell spacing of 3 m along the center of all major floodplain channels. In the Czuba et al. (2019) model (what we refer to as the original model), the nominal orthogonal cell spacing for the entire model domain was 15 m, with added breaklines refining the grid along the river channel centerline and banks to 12 m and along selected major floodplain channels and roadways to 3 m. The major improvement for the refined model used here is that some floodplain channels in the original model that had a nominal cell spacing of 15 m were now refined to 3 m. The locations of this refinement (where we added breaklines) traced the centerline of all floodplain channels that were inundated at a 1.2-months recurrence interval flow (382 m^3/s) when the major low-lying floodplain channels become inundated (Czuba et al., 2019). The refined computational mesh added over 163,000 new cells with a new total of 748,000 cells.

In the refined model, we maintained the original calibrated Manning's n-values. We compared model simulated and measured water-surface elevations and velocities for model validation. In the refined model, root-mean-square error (RMSE) and mean absolute error (MAE) was the same as the original Czuba et al. (2019) model. This suggests that our slight refinement of the model grid did not significantly affect water-surface elevations and velocities in the vicinity of our calibration and validation measurements partly because those floodplain channels had refined grids in the original model.

Model simulations were performed for the same 21 steady-state flow conditions as in Czuba et al. (2019). These flow conditions are referenced to the daily mean flow data at the USGS gage (03365500 East Fork

White River at Seymour, Indiana) for water years 1928–2019. From the model, we exported simulated depth, velocity, and bed shear stress for subsequent sediment transport analysis.

3.2. Analytical Methods

The simulated hydraulic data were used to estimate the largest (sediment particle) size that can be moved (LSM) in suspension or as bedload spatially across the river-floodplain at various flows. To find the LSM in suspension and as bedload we applied a Rouse number and a Shields stress mobility criterion, respectively. Simulated bed shear stresses were used to calculate Rouse number $\left(Z_R\right)$ and Shields stress (τ^*) for a wide range of expected sediment size classes transported in suspension and as bedload, 15 sizes in phi increments between 4 μm (very fine silt) and 64 mm (very coarse gravel; Garcia, 2008).

The LSM in suspension was computed by comparing the Rouse number $\left(Z_R\right)$ for a range of sediment sizes with a criterion for suspension. The Rouse number (Garcia, 2008) was calculated as

$$Z_R = \frac{w_s}{\kappa u_*}, \tag{1}$$

where κ is von Karman's constant (0.41), u_* is the shear velocity (m/s), and w_s is the sediment fall velocity (m/s), which is a function of particle diameter. We computed shear velocity $\left(u_*\right)$ from simulated bed shear stress as

$$u_* = \sqrt{\frac{\tau_b}{\rho}}, \tag{2}$$

where τ_b is the simulated bed shear stress (Pa) at each grid cell and ρ is the density of water (1,000 kg/m^3). Sediment fall velocity was calculated using the Ferguson and Church (2004) equation as

$$w_s = \frac{RgD^2}{C_1\upsilon + \sqrt{0.75\,C_2RgD^3}}, \tag{3}$$

where R is the submerged specific gravity (1.65), g is the gravitational acceleration (9.81 m/s^2), D is the sediment particle diameter using all 15 values in the range from 4 μm to 64 mm, υ is the kinematic viscosity of water (1×10^{-6} m^2/s), C_1 is a constant with a theoretical value of 18, and C_2 is a constant representing the asymptotic value of the drag coefficient ($C_2 = 1$ for natural grains).

For each grid cell at each flow (a single value of bed shear stress), we computed a Rouse number for each of our 15 sediment sizes. The Rouse number is a function of particle fall velocity and shear velocity. The threshold condition for a particle to remain in suspension is when the tendency for a particle to settle out of suspension (fall velocity) is balanced by turbulence acting to keep that particle in suspension (shear velocity). That is, when the fall velocity is equal to the shear velocity or, equivalently, when the Rouse number is equal to 2.43 ($1/\kappa$), which is the threshold value for a particle to remain in suspension (Engelund, 1965a, 1965b; Niño, 1995; Niño & García, 1998; Niño et al., 2003; Van Rijn, 1984). Therefore, the LSM in suspension was the largest sediment size (from the range of sediment sizes) for which $Z_R < 2.43$. Note that because the shear velocity is in the denominator and fall velocity is in the numerator of Equation 1, smaller values of Rouse number indicate a greater potential for suspension.

The LSM as bedload was computed by comparing Shields stress (τ^*) with critical Shields stress (τ_c^*) for a range of sediment sizes. At each flow, Shields stress (τ^*) was calculated as

$$\tau^* = \frac{\tau_b}{\rho g R D}, \tag{4}$$

where τ_b is the simulated bed shear stress at each grid cell (Pa), ρ is the density of water (1,000 kg/m^3), g is the gravitational acceleration (9.81 m/s^2), R is the dimensionless submerged specific gravity of a sediment particle (1.65), and D is the sediment particle diameter using all 15 values in the range from 4 μm to

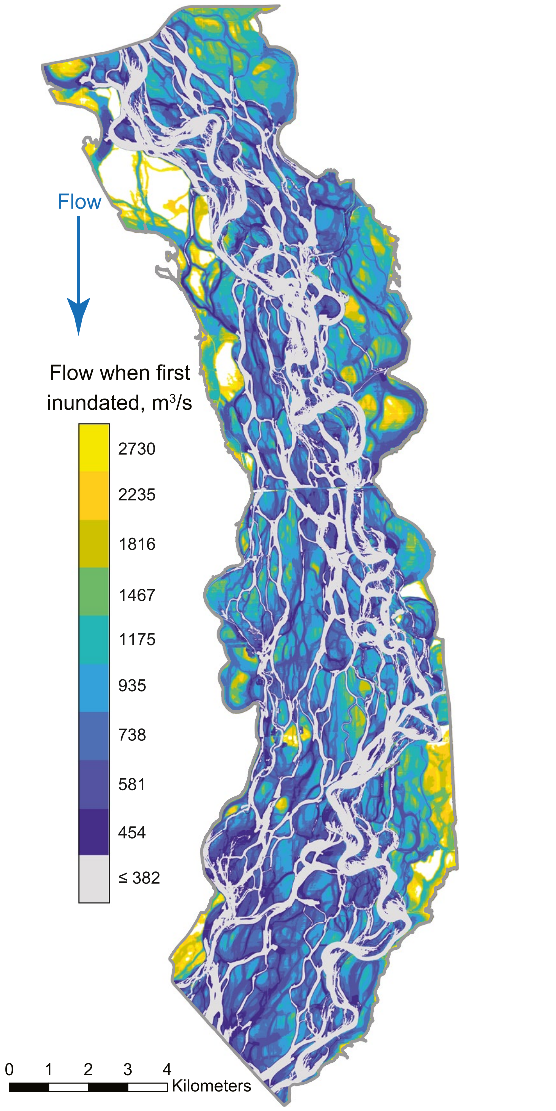

Figure 2. Flow at which the floodplain first becomes inundated. The area in light gray are those areas inundated at or below 382 m^3/s (1.2-month recurrence interval).

64 mm. Critical Shields stress (τ_c^*) was calculated for each sediment size as (Brownlie, 1981; Garcia, 2008)

$$\tau_c^* = \frac{1}{2}\left[0.22\,R_{ep}^{-0.6} + 0.06\exp\left(-17.77\,R_{ep}^{-0.6}\right)\right], \tag{5}$$

where R_{ep} is the particle Reynolds number expressed as

$$R_{ep} = \frac{\sqrt{gRD}\,D}{\upsilon}, \tag{6}$$

For each grid cell at each flow (a single value of bed shear stress), we computed a Shields stress and an associated critical Shields stress for each of our 15 sediment sizes. At locations where calculated $\tau^* > \tau_c^*$, that sediment size can be transported. Therefore, the LSM as bedload was the largest sediment size (from the range of sediment sizes) for which $\tau^* > \tau_c^*$.

The LSM at all flows was probabilistically integrated (based on flow recurrence) to compute an effective sediment size that can be moved in suspension and as bedload. This effective sediment size is similar to the idea of "effective discharge" proposed by Wolman and Miller (1960), where instead of integrating over flow magnitude and frequency (in the case of effective discharge), we replace flow magnitude with LSM. We call this effective grain size the Probabilistic Flow Integrated Grain Size (PFIGS) and calculate it as

$$\text{PFIGS} = \sum_i \text{LSM}_i P_i, \tag{7}$$

where LSM_i is the LSM at the i^{th} flow and P_i is the probability of occurrence of the i^{th} flow. The integration (summation in this discrete case) is over all i flows that inundate each grid cell and the probabilities must first be normalized at each grid cell such that $\sum P_i = 1$. For the 21 simulated flows for the EFWR, the 12$^{\text{th}}$ flow (382 m^3/s, 1.2-months r.i.) is the flow when the majority of low-lying floodplain channels first become inundated and fully connected. The flow at which each grid cell is first inundated is shown in Figure 2 and the integration for computing PFIGS at each grid cell only occurs at the flows at and above those shown in Figure 2. Therefore, our integration of LSM to calculate PFIGS was over 10 flow conditions (flows 12–21) or less.

3.3. Sediment Data

Suspended sediment was collected as single vertical samples from 6 locations in flowing floodplain channels and 2 locations in the river at bridges on May 1–2, 2017 using a DH-76 depth-integrating suspended hand-line sampler with 1-L plastic bottles or handheld DH-48 depth integrating sampler with 0.5-L bottles. At each location, 3–5 bottles of water and suspended sediment were collected by slowly lowering the sampler through the water column with a transit rate that collected a sufficient sample without overfilling the bottle (Edwards & Glysson, 1999). Suspended sediment concentration was determined using the evaporation method described in the ASTM International Test Method, D 3977—97(B) (see also Guy, 1969) and samples were composited to determine the particle size distribution with a Malvern Mastersizer® 3000E laser diffraction instrument.

Bed material was collected from the floodplain surface (44 locations) and a river bar (3 locations) on August 12, 2019. Floodplain samples were collected using a steel ring (4.76 cm diameter × 5.08 cm height) pounded

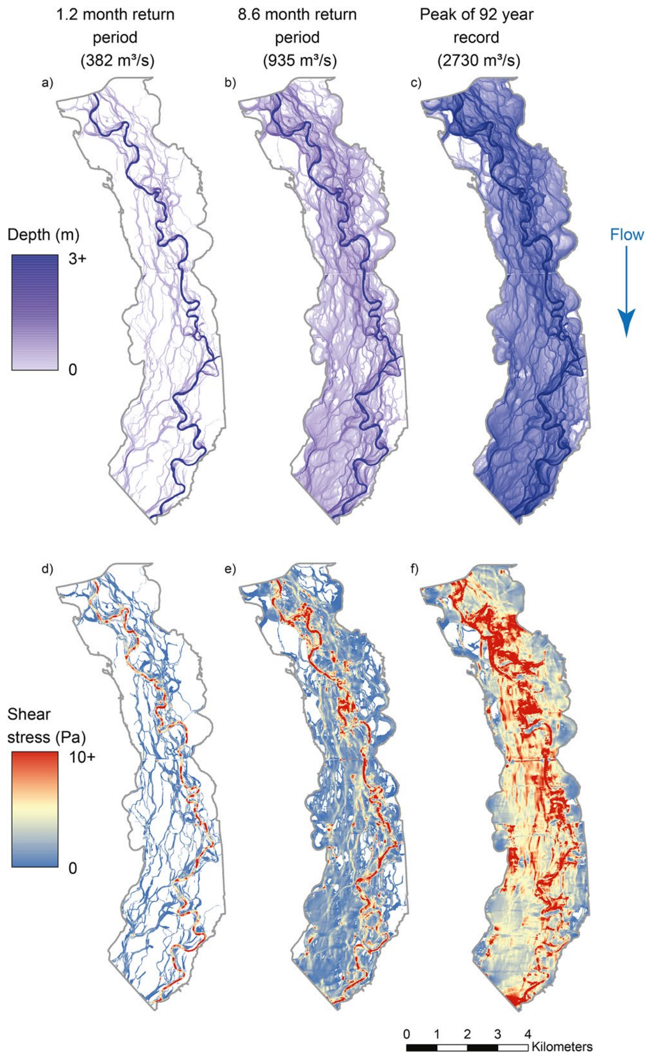

Figure 3. Simulated (a, b, c) depth and (d, e, f) bed shear stress for the high-frequency (a, d; 382 m^3/s), intermediate-frequency (b, e; 935 m^3/s) and low-frequency (c, f; 2,730 m^3/s) floods. The river channel can be seen as the darkest blue meandering line in (a).

into the surface to retrieve a 90 cm^3 sample of sediment (roughly 120 g of sediment per sample). Samples from the river bar were collected using a metal trowel to scoop up the top few centimeters of sediment over a local area large enough to fill a gallon-sized plastic bag (roughly 5.6 kg of sediment per sample). In the lab, all sediment samples were air dried. Floodplain sediment samples were additionally placed in a furnace at 400°C for a minimum of 4 h to incinerate any organics. Then all samples were sieved using sieves in phi-size gradations (Garcia, 2008) down to 62.5 μm to determine a particle size distribution.

Suspended sediment concentration (SSC) and some grain size information (percent finer than 62.5 μm) was downloaded from the USGS gage (03365500 East Fork White River at Seymour, Indiana; USGS, 2020). These data were collected between 1964 and 1981, following established USGS procedures for sediment data collection described in Edwards and Glysson (1999). The largest discharge for which SSC was measured was around 1,000 m^3/s, which has almost a 2-year recurrence interval. Each sample was marked as being on the rising or falling limb of the hydrograph and the season in which it was collected: Spring (March-May), Summer (June-August), Fall (September-November), and Winter (December-February). The only major difference between the methods used to collect our suspended sediment data and the USGS's data was that we collected suspended sediment from a single vertical location in each floodplain channel or river channel, whereas the USGS data were a composite of several verticals across the river channel.

3.4. Error Estimation

Errors of the predicted sediment sizes were calculated using MAE, RMSE, normalized mean absolute error (NMAE), normalized root mean square error (NRMSE), and relative root mean square error (RRMSE) methods. The MAE method calculates the average of individual differences and RMSE method estimates average magnitude of the error. The NMAE and NRMSE are calculated by dividing the MAE and RMSE by the average of the observed value, respectively. The equation for the RRMSE (Despotovic, et al., 2016) is

$$\mathrm{RRMSE} = \sqrt{\frac{1}{n}\sum_{i=1}^{n}\frac{\left(y_i - x_i\right)^2}{\left(y_i\right)^2}} \times 100 \, , \tag{8}$$

where y_i is the observed value and x_i is the predicted value.

4. Results

4.1. Simulated Depth and Shear Stresses

We highlight results at three important flow conditions for the EFWR: (high-frequency flood) at a 1.2-month recurrence interval flow (382 m^3/s), where the majority of the floodplain channels become inundated and convey roughly 25% of the total flow (Figure 3a); (intermediate-frequency flood) at an 8.6-month recurrence interval flow (935 m^3/s), where the floodplain is mostly inundated and conveys roughly 50% of the total flow (Figure 3b); and (low-frequency flood) at the peak flow of the 92-year USGS gaging record (2,730 m^3/s), where the floodplain is fully inundated and conveys roughly 75% of the total flow (Figure 3c; floodplain conveyance percentages from Czuba et al., 2019).

Inundation depth increases with increasing flow, with the deepest depths on the floodplain in floodplain channels (Figures 3a–3c). Bed shear stress increases with increasing flow and increasing depth (Figures 3e and 3f). For the high-frequency flood, floodplain channels only first become inundated and begin conveying flow with low bed shear stress compared to the river (Figure 3d). Between these floodplain channels are floodplain islands (Figures 3a and 3d), which are areas of relatively higher floodplain elevation that are inundated less frequently. For the intermediate-frequency flood, bed shear stress increases further in floodplain channels and is low on previous floodplain islands that are now inundated (Figure 3e). Many locations with locally high bed shear stress (small red patches, Figure 3e) are where flow in a floodplain channel overtops a farm road. For the low-frequency flood, bed shear stress in major floodplain channels and at floodplain valley constrictions is similar to the river channel (Figure 3f).

4.2. LSM in Suspension and as Bedload

LSM in suspension and LSM as bedload were calculated and will be described for the entire AOI. But first, we describe our results along a flowpath from the river and into two different floodplain channels as a detailed example demonstrating our calculations. Rouse numbers along the flowpath (one curve for each sediment size at each flow) are spatially and temporally variable (Figures 4a–4c). Rouse numbers substantially decrease transitioning from the river to FPC-1 for the high-frequency flood (Figure 4a), but are roughly constant for the low-frequency flood (Figure 4c). The sediment size corresponding to the curve just above the threshold line in Figures 4a–4c corresponds to the LSM in suspension (Figures 4d–4f).

The LSM in suspension increases with increasing flow in floodplain channels but remains constant at 125 μm in the river channel (Figures 4d–4f). This is likely because the high-frequency flood is still a relatively high flow in the river channel where increases in flow progressively spill across larger extents of the floodplain and do not contribute to large increases in shear stresses in the river channel (McKean & Tonina, 2013). In FPC-1, the substantial decrease in Rouse number for the high-frequency flood results in an LSM in suspension of only 16 μm whereas in FPC-2 the LSM increases to a constant 62 μm (Figure 4d). As flow increases, the LSM in suspension in the floodplain channels progressively increases, nearly to the same value as in the river (125 μm) for the low-frequency flood (Figures 4e and 4f). This indicates that there is a potential for the sediment in suspension in the river (finer than 125 μm) to enter FPC-1 for the low-frequency flood and subsequently fall out of suspension (coarser than 16 μm for the low-frequency flood and 62 μm for the intermediate-frequency and low-frequency floods; Figures 4d–4f). However, for the low-frequency flood, there is the greatest potential for any sediment supplied by the river to be carried in suspension across the floodplain (LSM in suspension in floodplain nearly a constant 125 μm; Figure 4f).

Compared to the Rouse number (Figures 4a–4c), Shields stress along the flowpath has more pronounced undulations (Figures 5a–5c). For the high-frequency flood, Shields stress is highest in the river channel, and decreases substantially in FPC-1 before increasing in FPC-2 (Figure 5a). As flow increases, Shields stress becomes more uniform across the river channel, FPC-1, and FPC-2 (Figures 5a–5c). The sediment size corresponding to the Shields stress curve just above its critical Shields stress threshold line in Figures 5a–5c is the LSM as bedload (Figures 5d–5f).

For the high-frequency flood, the river can move medium gravel (8–16 mm) as bedload, whereas FPC-1 can only move 2 μm as bedload (the lowest size considered) and FPC-2 can move up to 2 mm as bedload (Figure 5d). In FPC-1 at this same flow, the LSM in suspension is fine silt (16 μm; Figure 4d). The LSM in suspension in FPC-1 (Figure 4) is larger than the LSM as bedload in FPC-1 (Figure 5) because our formulation does not account for entrainment of fine sediment from the bed (Lamb & Venditti, 2016; Niño et al., 2003; Van Rijn, 1984), but rather focuses on whether sediments already in suspension will settle out (i.e., where would sediments already suspended in the river settle out once they enter the floodplain). For this high-frequency flood, FPC-1 is likely depositional because the LSM in suspension is much higher than the LSM as bedload. Coarse gravel (16–32 mm) can move in the river for the intermediate-frequency and low-frequency floods, whereas very coarse sand (1 mm) and fine gravel (4 mm) can move in FPC-1 and fine gravel (4–8 mm) and coarse gravel (16 mm) can move in FPC-2 for the intermediate-frequency and low-frequency floods, respectively (Figures 5e and 5f).

10.1029/2020WR028852

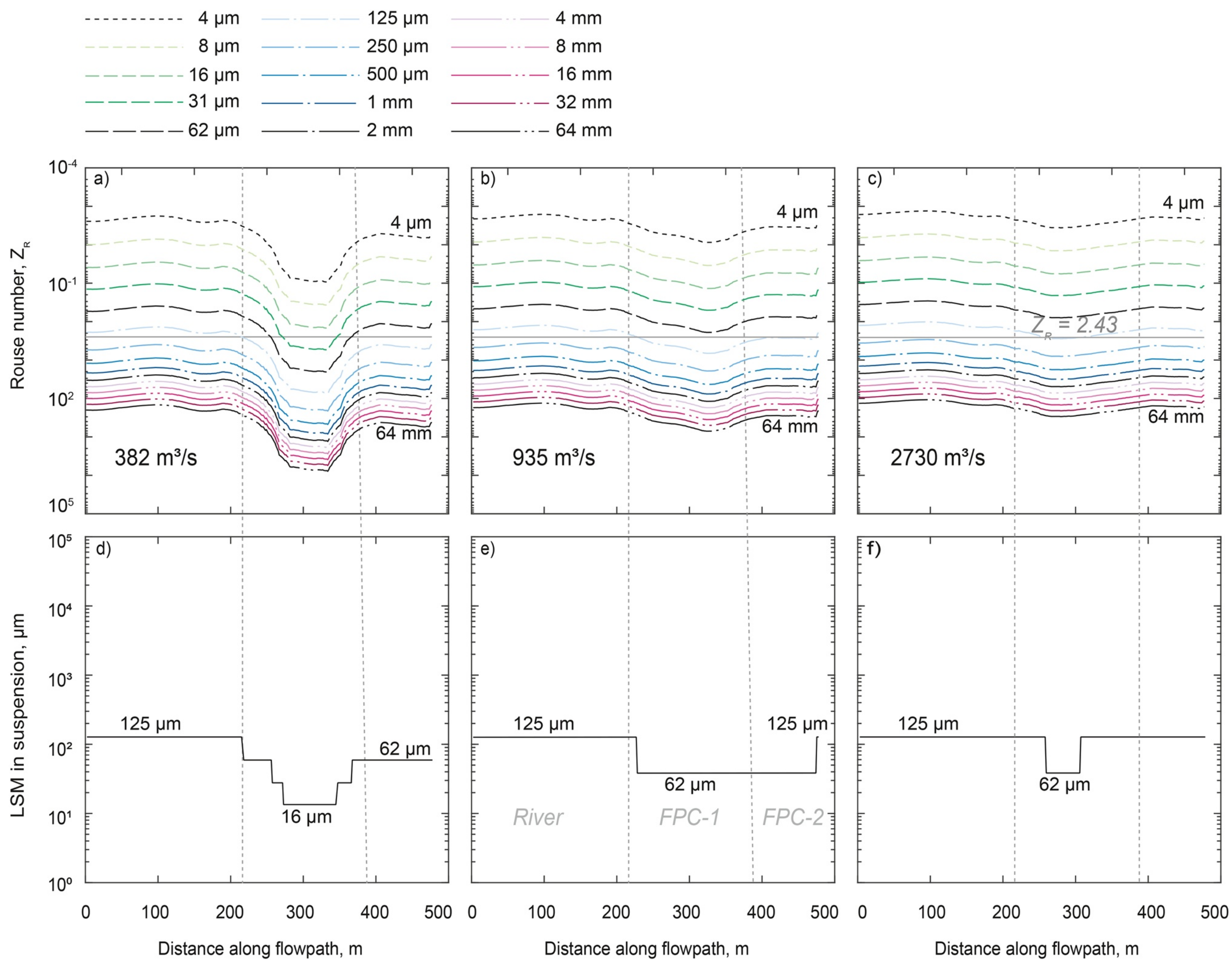

Figure 4. Largest size that can be moved (LSM) in suspension at three flows along the flowpath. Curved dashed lines trace the Rouse number along the flowpath (Figure 1c) for 15 sediment sizes for the (a) high-frequency (382 m^3/s), (b) intermediate-frequency (935 m^3/s), and (c) low-frequency (2,730 m^3/s) floods. Solid horizontal lines represent the Rouse number suspension threshold ($Z_R = 2.43$). Curved dashed lines above the solid line represent sediment sizes moved in suspension ($Z_R < 2.43$; note the *y*-axis is inverted). Vertical dashed lines show the break points among the river and floodplain channels (FPC-1 and FPC-2). FPC-1 is oriented transverse to the river and FPC-2 is oriented parallel to the river. Solid lines denote the LSM (μm) in suspension along the flowpath for the (d) high-frequency, (e) intermediate-frequency, and (f) low-frequency floods.

An LSM was calculated at each grid cell of the AOI, which represents the largest sediment particle size that can be moved in suspension or as bedload in a specific location at a specific flow. The largest of all values spatially across the AOI of LSM in suspension for the high-frequency and intermediate-frequency floods in the river channel is fine sand (125 μm). However, the largest of all values of the LSM for the low-frequency flood in the river channel and across the floodplain at all simulated discharges was medium sand (250 μm) (Figures 6a–6c). The most common LSM in suspension (based on largest percentage of area) for both river and floodplain for the high-frequency and intermediate-frequency floods was very fine sand (62 μm) (Figures 6a and 6b). Very fine sand (62 μm) could be transported in suspension in 73% and 92% of the wetted floodplain area and 66% and 94% of the river area for the high-frequency and intermediate-frequency floods, respectively. For the low-frequency flood, the most common sediment size in suspension was fine sand (125 μm), which could be transported in 74% of the wetted floodplain area and 77% of the river area. This shows, consistent with the findings from Figure 4, that the LSM in suspension is greater in the river than floodplain for the high-frequency flood and as flow increases, the LSM in suspension in the river and floodplain is similar.

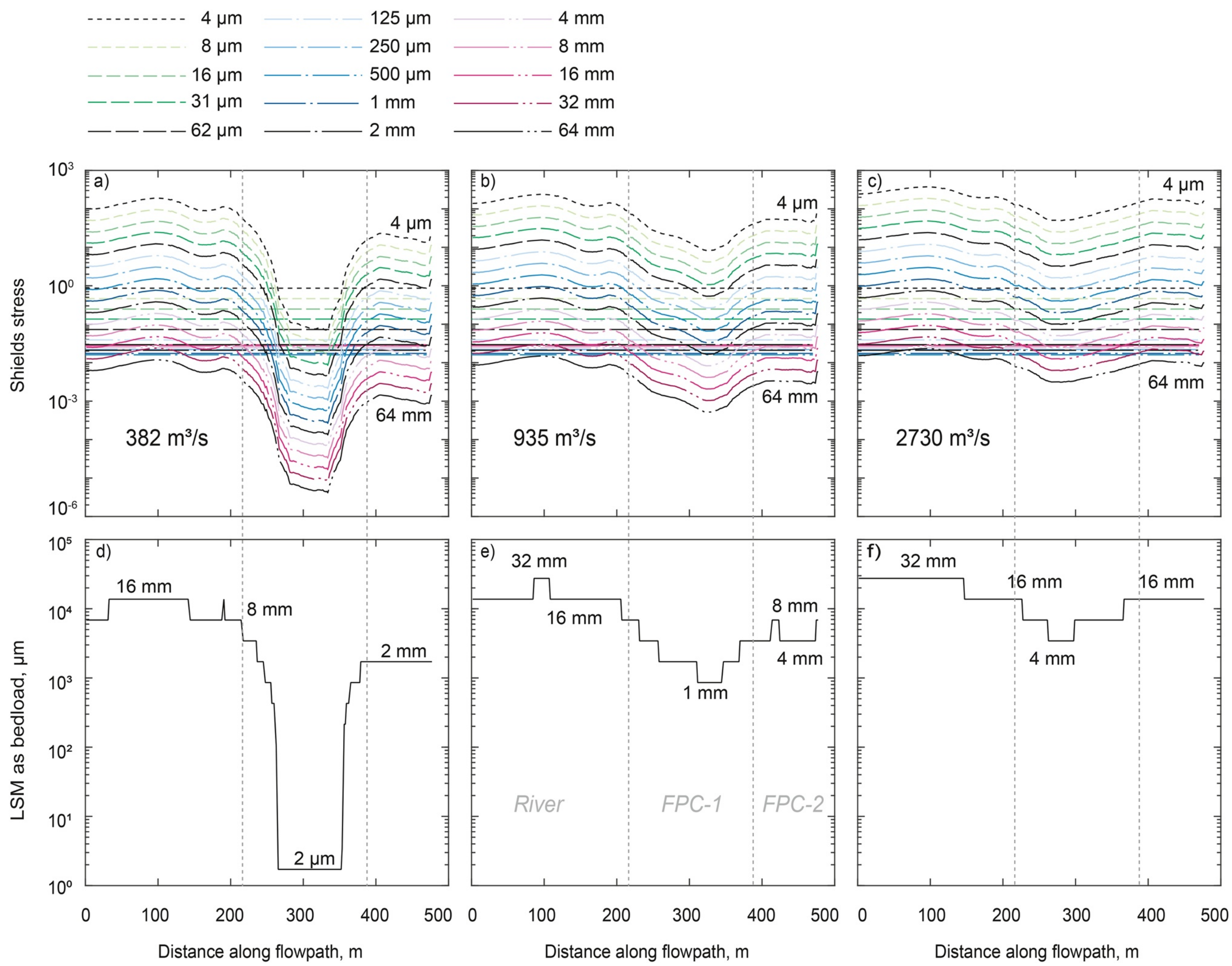

Figure 5. Largest size that can be moved (LSM) as bedload at three flows along the flowpath. Shields stress (τ^*, curved dashed lines) and corresponding critical Shields stress (τ_c^*, horizonal dashed lines) along the flowpath (Figure 1c) for 15 sediment sizes for the (a) high-frequency (382 m^3/s), (b) intermediate-frequency (935 m^3/s), and (c) low-frequency (2,730 m^3/s) floods. Curved dashed lines above their corresponding horizontal dashed line represent sediment sizes moved at least as bedload ($\tau^* > \tau_c^*$). Vertical dashed lines show the break points among the river and floodplain channels (FPC-1 and FPC-2). Solid lines denote the LSM (μm) as bedload along the flowpath at (d) high-frequency, (e) intermediate-frequency, and (f) low-frequency floods.

The largest of all values spatially across the AOI of LSM as bedload for all three flows was very coarse gravel (32 mm), however, the area of the river-floodplain that can move this size particle is very small. The most common LSM as bedload (based on largest percentage of area) for both the river and floodplain for the high-frequency, intermediate-frequency, and low-frequency floods are 2, 4, and 8 mm, respectively. These LSM can be transported as bedload in 54% of river and 64% of floodplain areas (2 mm) for the high-frequency flood, 56% of river and 62% of floodplain areas (4 mm) for the intermediate-frequency flood, and 82% of river and 78% of floodplain areas (8 mm) for the low-frequency flood (Figures 6d–6f). Some discrete patches of the floodplain can transport larger particles (32–64 mm) than in the river channel because of locally high bed shear stresses (Figure 3) where flow in floodplain channels overtops farm roads. At these locations, we have found angular gravel (∼2 cm diameter) washed from farm roads downstream into floodplain channels.

We have further summarized the data in Figure 6 as percentiles of LSM (25th, 50th, and 75th) in suspension in the river and as bedload on the floodplain (Figure 7). These summary statistics represent characteristics of the spatial distribution of LSM at each flow. We focus on suspended sediment in the river because those grains are supplied to the floodplain and bedload in the floodplain because that limits that largest size transported across the floodplain. At the lowest flows considered, the 25th percentile LSM as bedload on

10.1029/2020WR028852

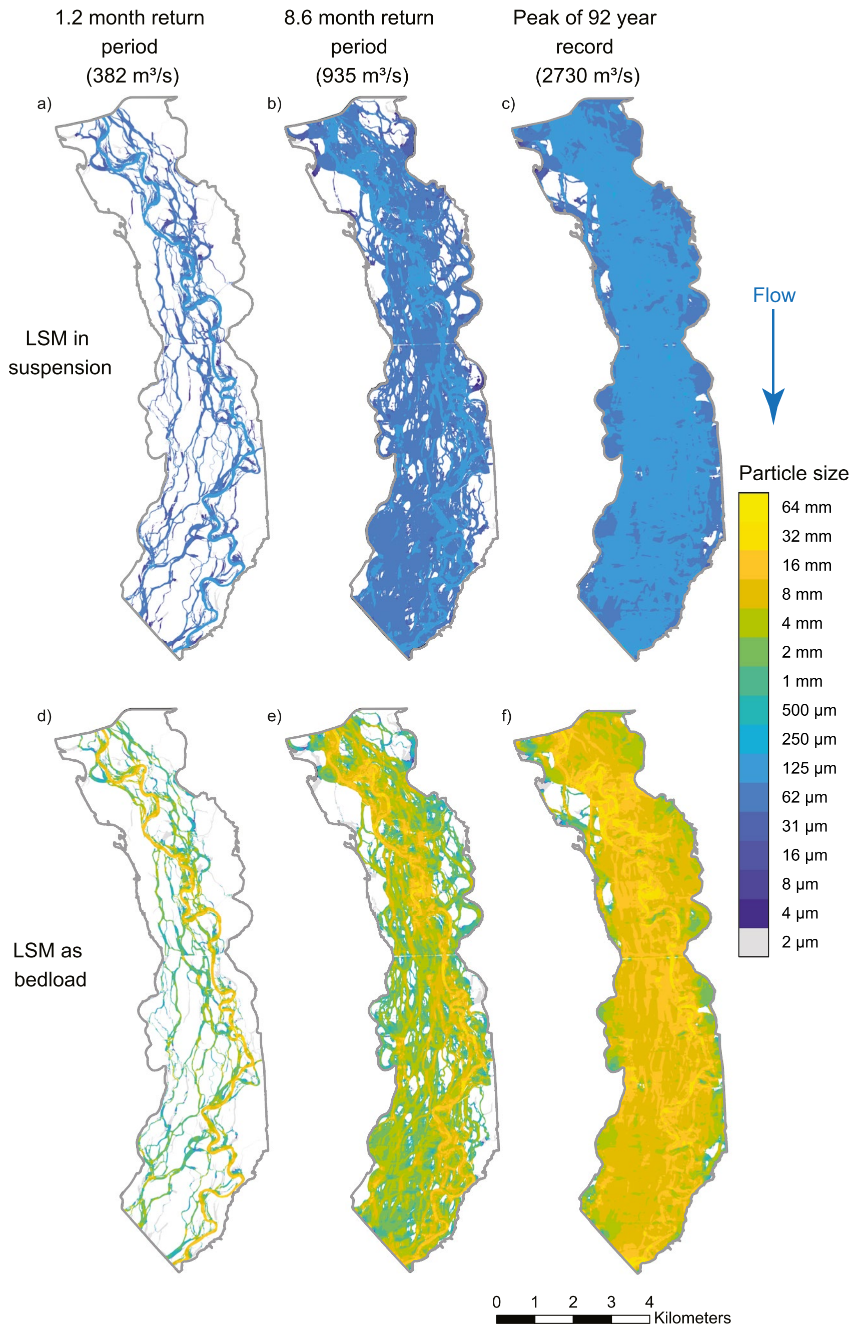

Figure 6. Largest size that can be moved (LSM) in suspension (a)–(c) and as bedload (d)–(f) within an area of interest (AOI) for the high-frequency (a, d; 382 m^3/s), intermediate-frequency (b, e; 935 m^3/s), and low-frequency (c, f; 2,730 m^3/s) floods.

the floodplain is 2 μm and lower than that for suspended sediment (Figure 7, see also previous discussion of FPC-1 in the context of Figures 4 and 5: Section 4.2, paragraph 4). These are locations where segments of floodplain channels are wet, likely from backwater, but are not conveying flow. These locations can be seen in Figure 6 when comparing the gray segments of floodplain channels in Figure 6d with corresponding locations in Figure 6a that are blue. For the high-frequency and intermediate-frequency floods, the LSM in suspension in the river is nearly constant at 62 μm, increasing to 125 μm only at the highest flows (Figure 7). In comparison, the 50th percentile LSM as bedload on the floodplain increases by nearly an order of magnitude, from 1 to 8 mm (Figure 7). These data clearly show that the EFWR is capable of suspending

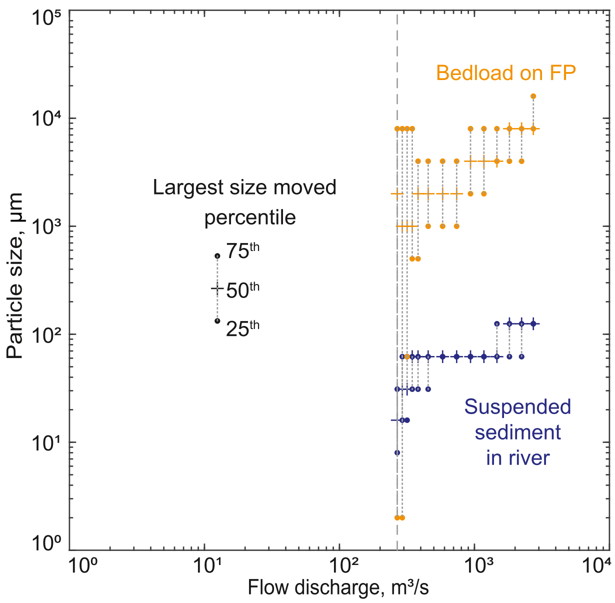

Figure 7. Percentiles (25th, 50th, and 75th) of LSM (μm) in suspension in the river (blue) and as bedload on the floodplain (orange). These summary statistics represent characteristics of the spatial distribution of LSM at each flow. Dashed line represents the activation of floodplain channels.

and supplying sediment as coarse as sand to the floodplain, but the floodplain, in general, and floodplain channels, specifically, have the capacity to transport gravel (Figure 7).

4.3. Effective Grain Size or PFIGS

From our LSM analysis, larger particles could be transported over large areas during low-frequency floods and smaller particles could be transported over small areas during high-frequency floods. Therefore, to probabilistically integrate the LSM into an effective grain size, we developed and computed the PFIGS (Equation 7), which synthesizes the collection of LSM results at each flow into a single grain size that is most likely to play a key role in river-floodplain morphodynamics. In subsequent sections, we show that PFIGS is predictive of the D97 in suspension and D98 of bed surface material (characteristic of the largest sizes transported), and how together with field data can be used to assess net depositional versus erosional trajectory. The most common PFIGS in suspension (based on largest percentage of area) in the river is fine sand (125–250 μm), in floodplain channels and in remaining areas of the floodplain is very fine sand (62–125 μm; Figure 8a). These sediment sizes could be transported, by area, in 80% of the river (125–250 μm), in 70% of floodplain channels (62–125 μm), and across 62% of remaining areas of the floodplain (62–125 μm; Figure 8a). The 50th and 90th percentile (spatially) PFIGS in suspension in the river is 81 and 115 μm, in the floodplain channel is 38 and 58 μm, and across the entire floodplain is 36 and 57 μm, respectively. The most common PFIGS as bedload (based on largest percentage of area) in the river is coarse gravel (16–32 mm) and in floodplain channels and in remaining areas of the floodplain is very fine gravel (2–4 mm; Figure 8b). These sediment sizes could be transported, by area, in 48% of the river (16–32 mm), in 83% of floodplain channels (2–4 mm), and across 59% of remaining areas of the floodplain (2–4 mm; Figure 8b). The 50th and 90th percentile (spatially) PFIGS as bedload in the river is 8 and 15 mm, in the floodplain channels is 1.7 and 4 mm, and across the entire floodplain is 1 and 2.8 mm, respectively.

4.4. Measured Suspended Sediment Data

Measured SSC, at a flow of ~454 m^3/s, was highest in the river (368 mg/L), decreased in floodplain channels proximal to the river (~100 mg/L), and decreased further in floodplain channels distal to the river (62–69 mg/L; Figure 9a). At this flow (454 m^3/s), fine silt (11.2 μm) had the highest relative frequency (mode) in the river, very fine silt (6.83 μm) in proximal floodplain channels, and coarse clay (3.75 μm) in the distal floodplain channels (zonal averages from Figure 9b). The measured D50 in suspension also decreased with increasing distance from the main channel; river: 16 μm (medium silt), floodplain channels proximal: 6.3 μm (very fine silt), and floodplain channels distal: 5.3 μm (very fine silt; Figure 9c). The sampling flow (454 m^3/s) is just above the high-frequency flood (382 m^3/s) and major floodplain channels are inundated at this flow. The decrease in SSC and suspended sediment size when comparing samples taken proximal to the river (a, b, c) with those farther into the floodplain (d, e, f), suggests that sediment is falling out of suspension from the river to distal floodplain channels.

Suspended sediment characteristics measured in the river at the USGS gage are shown in Figure 10. The variability in SSC decreases at a flow of 268 m^3/s (Figure 10a), which is when the most low-lying floodplain channels first become inundated or activated (Czuba et al., 2019). This may be due to the floodplain (and floodplain channels specifically) modulating SSC in the river or it could be due to a lack of sampling at higher flows. As flow increases above 268 m^3/s, the SSC in the river may plateau or continue to increase slightly. For context, we also show measured SSC in regards to the rising and falling limb and season (Figure 10a). But again, due to the lack of sampling across a range of flows (particularly for the data on the rising limb) we do not attempt any statistical analyses of this data set. Most sediment in suspension in the river at the USGS gage is fines (finer than 62.5 μm; Figure 10b). There is no clear pattern in percent fines measured in

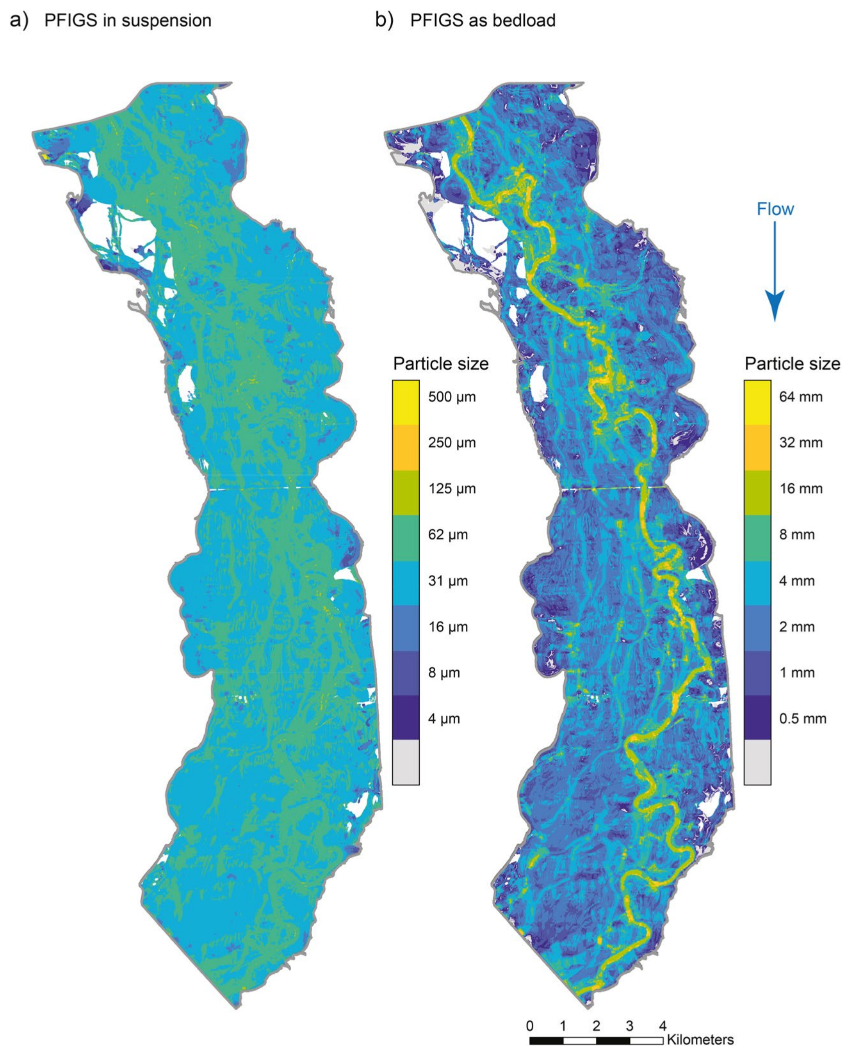

Figure 8. Effective sediment size or Probabilistic Flow Integrated Grain Size (PFIGS) in suspension (a) and as bedload (b) within the area of interest (AOI). Note panels (a) and (b) have different color bar scales.

regards to flow, the rising and falling limb, or season from these measurements (Figure 10b). This may in part be due to the presence of a low-head dam just upstream of the USGS gage that likely traps some sand (see description and location in Czuba et al., 2019).

4.5. Comparison of PFIGS with Measured Data

We compared our predicted PFIGS grain sizes with a range of grain sizes from measured distributions (D50-D99). Suspended sediment in the river (1 location) and floodplain (6 locations) were compared with PFIGS and LSM in suspension at the sampling flow (454 m^3/s). The D97 in suspension from measured data in the floodplain best agreed with PFIGS and the LSM in suspension at the sampling flow (PFIGS: 0.04 mm MAE, 0.06 mm RMSE, 32% NMAE, 49% NRMSE, and 35% RRMSE; LSM: 0.04 mm MAE, 0.05 mm RMSE, 38% NMAE, 46% NRMSE, and 47% RRMSE; $n = 6$ excluding the river sample; Figure 11). At one distal floodplain channel location ("f" in Figure 9a), D90 was the best match with PFIGS and LSM in suspension, and in the river, D85 was the best match with PFIGS and D86 was the best match with LSM. Best matches of measured suspended sediment percentile sizes with PFIGS and LSM in suspension ranged from D94 to D99 (PFIGS: 2 MAE, 3.3 RMSE; LSM: 1.8 MAE, 3 RMSE; $n = 6$ excluding river sample).

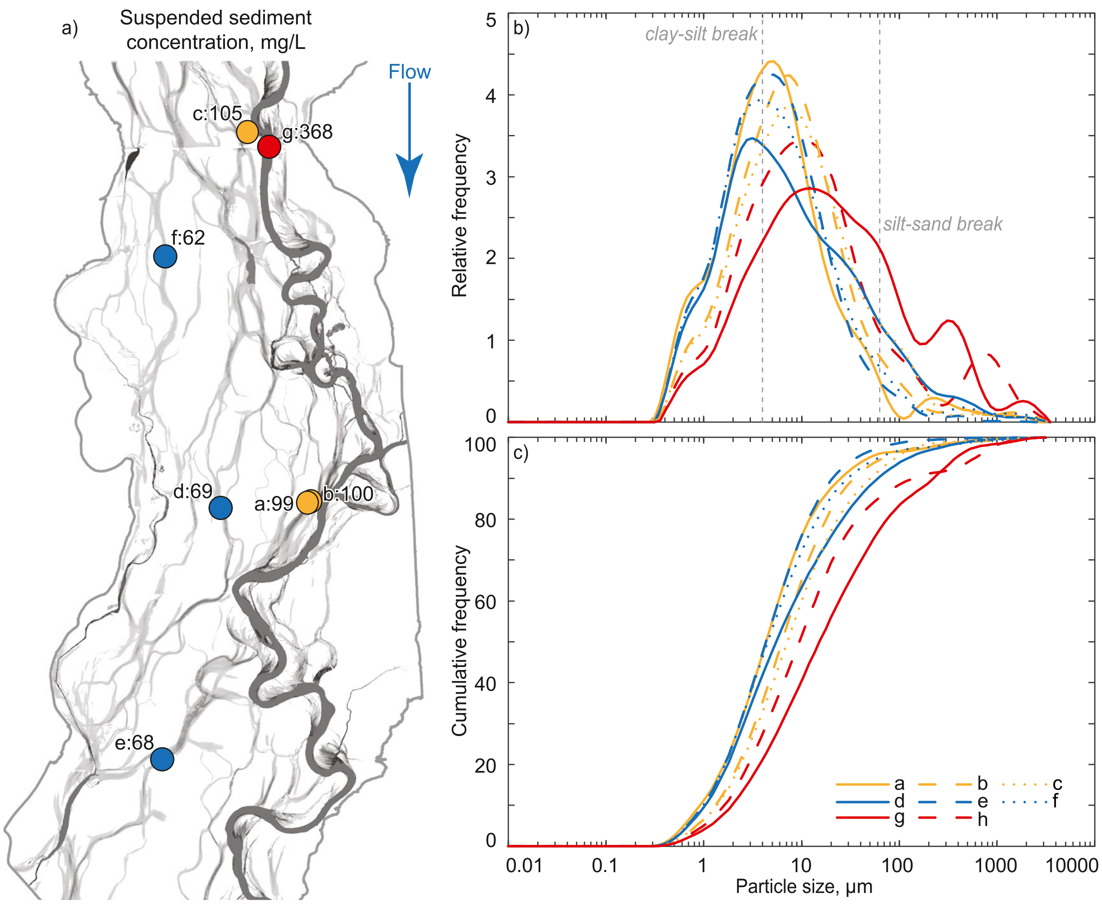

Figure 9. Measured suspended sediment in the East Fork White River and its floodplain, in Indiana at eight sampling locations collected on May 1–2, 2017. Red, orange, and blue colors represent the sampling locations in the river, in floodplain channels proximal to the river, and in floodplain channels distal to the river, respectively. (a) Suspended sediment concentration (mg/L) at seven locations (one location, "h," is farther downstream). The gray colors are model simulated depths at the approximate conditions (454 m^3/s) when the data were collected. (b) Size distribution of suspended sediment (μm). First dashed line is the clay-silt break (4 μm) and second dashed line is the silt-sand break (62.5 μm). (c) Cumulative particle size distribution of suspended sediment (μm).

The D98 from measured bed material samples best agreed with PFIGS as bedload (PFIGS: 3.6 mm MAE, 6.9 mm RMSE, 83% NMAE, 157% NMAE, and 97% RRMSE, $n = 47$; Figure 11). The D98 of measured bed material spans nearly two orders of magnitude (449 μm–16 mm; Figure 11). The two locations farthest to the right (in Figure 11) where PFIGS is over estimating the sediment sizes are on the bank of the river where close proximity to the river, in the model, leads to a high PFIGS. Other sources of variability included a few locations with randomly larger particles (gravel) in the sample (highest orange circles above the 1:1-line, Figure 11; here D75 was generally the best match with PFIGS) and a few locations likely affected by backwater, just upstream of a roadway culvert, for instance (lowest orange circles below the 1:1-line, Figure 11). Including all the variability of all locations, D98 is the best match with PFIGS as bedload, ranging from D90 to D99, and with a 2.4 MAE and 4.5 RMSE ($n = 47$).

5. Discussion

The EFWR is capable of regularly suspending sediment (the largest size for which the Rouse number, Z_R < 2.43) as coarse as sand (62–125 μm; Figure 7) high enough in the water column to overtop the river bank and supply the floodplain (Figure 9, locations a, b, c). While we do see coarser sands in suspension in the river (Figure 9b), these sediments are likely suspended lower in the water column and are not as easily lifted sufficiently high in suspension. During high-frequency floods, the supplied suspended sediment from the river to the floodplain can easily fall out of suspension as the transport capacity is much lower on the floodplain (Figures 4 and 9). These first flows that inundate the floodplain may be capable of modulating the

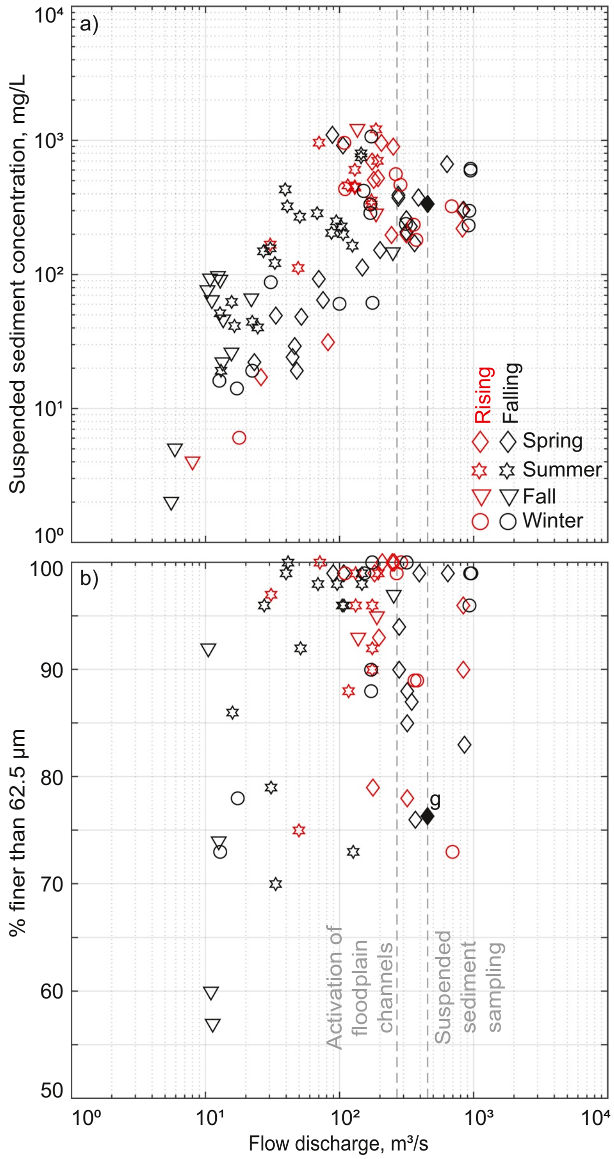

Figure 10. Suspended sediment measured at USGS streamflow-gaging station 03365500 East Fork White River at Seymour, Indiana (~5.7 km along the channel centerline downstream from the AOI). (a) Suspended sediment concentration (mg/L) and (b) percent fines (finer than 62.5 μm) on the rising (red) and falling (black) limb of the hydrograph during different seasons (symbols). Solid black diamond shows the value measured in the river at sampling location "g" (from Figure 9) at a flow of 454 m^3/s. First dashed line represents the activation of floodplain channels (268 m^3/s; Czuba et al., 2019) and second dashed line indicates the flow (454 m^3/s) representative of conditions at the time of suspended sediment sampling (Figure 9).

SSC in the river (Figure 10a). We hypothesize that this could occur by the exchange of water from the river to the floodplain, with sediment deposition, and then that water returning back to the river, where this occurs many times over a long reach with many floodplain channels. It is beyond the scope of this study to delve further into this hypothesis, but we leave it for future work with perhaps more field data collection or a morphodynamic model. As flow increases, the SSC in the river may be increasing, however more data are necessary to say with statistical confidence (Figure 10a). This could occur because with increasing flow the fraction of suspended sediment depositing on the floodplain decreases, allowing for more suspended sediment to pass over the floodplain and return back to the river, thereby progressively lessening dilution of the SSC in the river. At the highest observed flow, the flow over the floodplain can suspend and convey the 125 μm sediment sizes supplied by the river, essentially passing this sediment across the floodplain with little potential for deposition (Figures 4f and 6c). To summarize, fine sediment suspended in the river can deposit on the floodplain during high-frequency floods, but during low-frequency floods, more of the supplied sediment can remain suspended as it passes over the floodplain.

At the same time, these floodplain channels are highly efficient at transporting sediment, and model results suggest that sediment sizes up to 1–8 mm (Figure 7) can readily be transported as bedload. In the field, at locations where gravel farm roads cross floodplain channels, we have found angular gravel (~2 cm diameter) washed downstream in floodplain channels. These floodplain channels clearly are capable of transporting gravel. This means that any sediment that falls out of suspension in a floodplain channel could still move along the bed. Furthermore, PFIGS as bedload is predictive of the D98 of the surface of floodplain channels (Figure 11). This suggests floodplain channels are supply limited and the grain size distribution of the bed surface is set by the flow conditions (Buffington & Montgomery, 1999; Dietrich et al., 1989; Nelson et al., 2009). If the floodplain channels were transport limited, then the grain size distribution would be strongly related to the grain size distribution of the sediment supply (much finer) and not floodplain surface hydraulics (i.e., via PFIGS) (Buffington & Montgomery, 1999; Leopold, 1992; Nolan & Marron, 1995; Rice, 1994). Therefore, floodplain channels that are supply limited are most likely erosional.

It is possible that the cumulative deposition during high-frequency floods could counteract erosion during low-frequency floods, leading to net deposition in floodplain channels. We did not try to quantity the amount of fine sediment that falls out of suspension on the floodplain during high-frequency floods. However, if fine sediment deposition was overwhelming erosion, then the surface grain size should be much finer and not reflective of the LSM/PFIGS as bedload. Therefore, we conclude that the floodplain channels of the EFWR are net erosional. Though, morphodynamic simulations and additional field measurements would help to confirm this conclusion.

A limitation of this analysis is that we do not fully account for flow-vegetation-sediment interactions. In the 2-D HEC-RAS model, vegetation was only accounted for by a Manning's roughness value based on the National Land-Cover Database. Therefore, most of the floodplain is treated as agricultural lands with a calibrated n-value of 0.050 (Czuba et al., 2019). The National Land-Cover Database has a 30-m resolution and, in general, is not sufficient to characterize the variation in vegetation types we see in the field: floodplain

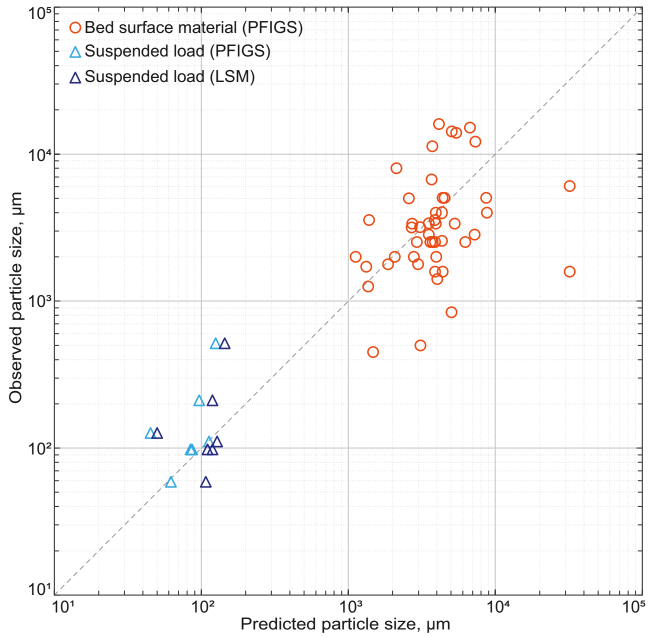

Figure 11. Comparison of predicted and observed sediment sizes (µm). PFIGS in suspension (light blue triangles) and LSM at the sampling flow (dark blue triangles; 454 m^3/s) (7 sampling locations) shows good agreement with measured suspended sediment D97. PFIGS as bedload shows good agreement with the D98 (orange circles) of measured floodplain surface (44 sampling locations) and river bar (3 locations). Sampling locations cover a wide range of topographic variation including floodplain channels, depressions, and islands and river bar. See Figure 1b for sampling locations. LSM, Largest size that can be moved; PFIGS, Probabilistic Flow Integrated Grain Size.

channels with corn, soybeans, barren, grass, and weeds. Furthermore, this does not account for the seasonal changes where floodplain channels planted with corn and soybeans are barren with some crop residue in the winter and early spring when some of the highest flows can occur. We interpret our results as being most applicable to floodplain channels that are barren or seasonally barren. It is likely that perennial vegetation in floodplain channels would further dampen flow momentum (not accounted for in the 2-D HEC-RAS model) and promote sediment deposition. Fully exploring this dynamic is a future research direction.

An important advancement presented in this paper is the idea of an effective grain size that is computed as the PFIGS. The effective grain size translates the idea of an effective discharge (Wolman & Miller, 1960) to sediment size and indicates a morphodynamically important grain size assuming the grain size distribution is set by flow hydraulics. With accompanying floodplain surface sediment size data (Figure 11), we were able to assess whether this floodplain, and the floodplain channels specifically, are on a net erosional or depositional trajectory. By computing the PFIGS as bedload, we were able to predict the upper end of the grain size distribution of the bed sediment in floodplain channels (D93 to D99). Additionally, by computing the PFIGS in suspension (and the LSM at the sampling flow), we were able to predict the upper end of the suspended sediment grain size distribution (D94 to D99). The effective grain size (PFIGS) probabilistically integrates the LSM. Therefore, the effective grain size represents the upper end of the grain size distribution for sediment in transport or on the bed. The D97 or D98 are sizes characteristic of the largest sizes measured. These sizes at the upper end of the grain size distribution are morphodynamically important because they are the "threshold" size, below which grains are easy to move and above which are more difficult to move. There may be an intermediate-frequency flood for which the PFIGS, and therefore all sizes on the bed, are fully mobile. The size of sediment supplied relative to this effective grain size will dictate whether that sediment is transported or deposited and lead to any subsequent morphodynamic change. This method is expected to be equally applicable to intermittently flooded coastal areas as well.

The EFWR is an end member of floodplains with channels that appear to be highly effective at transporting sediment. It would be interesting to apply the methods developed in analysis of this floodplain to other floodplains. For instance, in non-channelized floodplains where deposition is more prominent, we would expect to see the distributions of LSM as bedload on the floodplain and LSM in suspension in the river (Figure 7) with much less separation, more overlap, or perhaps flip-flopped in comparison to the EFWR. Such results would indicate a lower sediment transport capacity over the floodplain and confirm the method's utility across erosional to depositional floodplains. Then, the ultimate utility is in determining what set of conditions lead to floodplains with erosional versus depositional tendencies. This would also be valuable in designing floodplain restorations to assess the morphodynamic trajectory of engineered floodplain channels. Without fully accounting for all of the flow-vegetation-sediment feedbacks, the floodplain of the EFWR appears to be on a trajectory of continued maintenance of an anastomosing floodplain channel network that one day may serve as a river-avulsion pathway.

6. Concluding Remarks

We analyzed size-specific sediment transport potential and assessed whether the channelized floodplain of the East Fork White River near Seymour, Indiana, USA is on a net erosional or depositional trajectory. During high-frequency floods, the largest sediment size that can be moved in suspension in the river is larger than on the floodplain, but during low-frequency floods, the largest sediment size that can be moved in suspension in the river and on the floodplain are the same. Our results suggest that, during high-frequency floods, fine sediment suspended in the river can deposit on the floodplain, but during low-frequency floods, more of the supplied sediment can remain suspended as it passes over the floodplain. These floodplain channels can transport sand-size particles in suspension and gravel-size particles as bedload. This suggests that these floodplain channels could transport the sediment supplied by the river as bedload, which indicates that these floodplain channels are supply limited and the grain size distribution of the bed surface is set by the flow conditions. Supply limited floodplain channels are likely erosional. Finally, our proposed method of probabilistically integrating the largest sediment size that can be moved at various flows can be used to predict the upper end of the grain size distribution in suspension and in bed material, which is applicable to floodplains and coastal areas.

Data Availability Statement

Datasets for this research are available at: https://www.hydroshare.org/resource/79d8805a45d04a85ba519a7564e3700a/.

Acknowledgments

This work was partially supported by the Malcolm and Sylvia Boyce endowment made to Indiana University, and the Virginia Agricultural Experiment Station and USDA Hatch program (1017457). D. A. Edmonds acknowledges support from NSF Grant 1911321. The authors thank three anonymous reviewers, Associate Editor (Ryan Morrison), and Editor (Ellen Wohl) for providing thoughtful and insightful comments that helped improve the presentation of our work.

References

Allen, J. R. L. (1965). A review of the origin and characteristics of recent alluvial sediments. *Sedimentology*, *5*(2), 89–191. https://doi.org/10.1111/j.1365-3091.1965.tb01561.x

Bates, P. D., Anderson, M. G., Price, D. A., Hardy, R. J., & Smith, C. N. (1996). *Analysis and development of hydraulic models for floodplain flows* (pp. 215–254). Floodplain processes.

Benke, A. C., Chaubey, I., Ward, G. M., & Dunn, E. L. (2000). Flood pulse dynamics of an unregulated river floodplain in the southeastern U.S. coastal plain. *Ecology*, *81*(10), 2730–2741. https://doi.org/10.1890/0012-9658(2000)081[2730:FPDOAU]2.0.CO;2

Bristow, C. S., Skelly, R. L., & Ethridge, F. G. (1999). Crevasse splays from the rapidly aggrading, sand-bed, braided Niobrara River, Nebraska: Effect of base-level rise. *Sedimentology*, *46*(6), 1029–1047. https://doi.org/10.1046/j.1365-3091.1999.00263.x

Brown, A. G. (1996). Floodplain palaeoenvironments. In M. G. Anderson, P. D. Bates, & D. E. Walling (Eds.), *Floodplain processes* (pp. 95–138). Hoboken, NJ: Wiley.

Brownlie, W. R. (1981). Prediction of flow depth and sediment discharge in open channels Report No. KH-R-43A. Pasadena, CA: Keck Laboratory of Hydraulics and Water Resources, *California Institute of Technology*.

Buffington, J. M., & Montgomery, D. R. (1999). Effects of sediment supply on surface textures of gravel-bed rivers. *Water Resources Research*, *35*(11), 3523–3530. https://doi.org/10.1029/1999WR900232

Crawford, C. G., Lydy, M. J., & Frey, J. W. (1996). Fishes of the White River Basin, Indiana. *U.S. Geological Survey Water-Resources Investigations Report* (Vol. 8, pp. 96–4232). P. Reston, VA: U.S. Geological Survey.

Czuba, J. A., David, S. R., Edmonds, D. A., & Ward, A. S. (2019). Dynamics of surface-water connectivity in a low-gradient meandering river floodplain. *Water Resources Research*, *55*(3), 1849–1870. https://doi.org/10.1029/2018WR023527

David, S. R., Czuba, J. A., & Edmonds, D. A. (2019). Channelization of meandering river floodplains by headcutting. *Geology*, *47*(1), 15–18. https://doi.org/10.1130/G45529.1

David, S. R., Edmonds, D. A., & Letsinger, S. L. (2017). Controls on the occurrence and prevalence of floodplain channels in meandering rivers. *Earth Surface Processes and Landforms*, *42*(3), 460–472. https://doi.org/10.1002/esp.4002

Despotovic, M., Nedic, V., Despotovic, D., & Cvetanovic, S. (2016). Evaluation of empirical models for predicting monthly mean horizontal diffuse solar radiation. *Renewable and Sustainable Energy Reviews*, *56*, 246–260. https://doi.org/10.1016/j.rser.2015.11.058

Dietrich, W. E. (1987). Mechanics of flow and sediment transport in river bends. In *River channels: Environment and process* (Vol. 18, pp. 179–227). Oxford: Blackwell.

Dietrich, W. E., Kichner, J. W., Ikeda, H., & Iseya, F. (1989). Sediment supply and the development of the surface layer in gravel bedded rivers. *Nature*, *340*(1975), 215–217. https://doi.org/10.1038/340215a0

Garcia, M. (Ed.). (2008). *Sedimentation engineering: Processes, measurements, modeling, and practice*. American Society of Civil Engineers.

Edwards, T. K., & Glysson, G. D. (1999) *Field methods for measurement of fluvial sediment* (Vol. 3, p. 89). Denver, CO: U.S. Geological Survey Techniques of Water-Resources Investigations.

Engelund, F. (1965a). A criterion for the occurrence of suspended load. *La Houille Blanche*, *8*(7).

Engelund, F. (1965b). *Turbulent energy and suspended load* (Vol. 10). Coastal Engineering Laboratory, Technical University of Denmark.

Fagan, S. D., & Nanson, G. C. (2004). The morphology and formation of floodplain-surface channels, Cooper Creek, Australia. *Geomorphology*, *60*(1–2), 107–126. https://doi.org/10.1016/j.geomorph.2003.07.009

Ferguson, R. I., & Church, M. (2004). A simple universal equation for grain settling velocity. *Journal of Sedimentary Research*, *74*(6), 933–937. https://doi.org/10.1306/051204740933

Guy, H. P. (1969). Laboratory theory and methods for sediment analysis. In *Techniques of water-resources investigations of the U.S. Geology. Survey*. (p. 55). Reston, VA. Retrieved from http://pubs.usgs.gov/twri/twri5c1/

Homer, C. G., Dewitz, J. A., Yang, L., Jin, S., Danielson, P., Xian, G., et al. (2015). Completion of the 2011 national land cover database for the conterminous United States—Representing a decade of land cover change information. *Photogrammetric Engineering & Remote Sensing*, *81*(5), 345–354.

Jackson, R. G. (1976). Depositional model of point bars in the lower Wabash River. *Journal of Sedimentary Petrology*, *46*, 579–594.

James, C. S. (1985). Sediment transfer to overbank sections. *Journal of Hydraulic Research*, *23*(5), 435–452. https://doi.org/10.1080/00221688509499337

Kleinhans, M. G., & van den Berg, J. H. (2011). River channel and bar patterns explained and predicted by an empirical and a physics-based method. *Earth Surface Processes and Landforms*, *36*(6), 721–738. https://doi.org/10.1002/esp.2090

Knight, D., & Shiono, K. (1996). River channel and floodplain hydraulics. In M. G. Anderson, P. D. Bates, & D. E. Walling (Eds.), *Floodplain processes* (pp. 139–182). Hoboken, NJ: Wiley.

Kupfer, J. A., Meitzen, K. M., & Gao, P. (2015). flooding and surface connectivity of Taxodium-Nyssa stands in a southern floodplain forest ecosystem. *River Research and Applications*, *31*(10), 1299–1310. https://doi.org/10.1002/rra.2828

Lamb, M. P., & Venditti, J. G. (2016). The grain size gap and abrupt gravel-sand transitions in rivers due to suspension fallout. *Geophysical Research Letters*, *43*(8), 3777–3785. https://doi.org/10.1002/2016GL068713

Lauer, J. W., & Parker, G. (2008). Modeling framework for sediment deposition, storage, and evacuation in the floodplain of a meandering river: Application to the Clark Fork River, Montana. *Water Resources Research*, *44*(8), 1–16. https://doi.org/10.1029/2006WR005529

Lauer, J. W., & Willenbring, J. (2010). Steady state reach-scale theory for radioactive tracer concentration in a simple channel/floodplain system. *Journal of Geophysical Research*, *115*(4), 1–21. https://doi.org/10.1029/2009JF001480

Leopold, L. B. (1992). Sediment Size that determines channel morphology. *Dynamics of Gravel-Bed Rivers*, 297–311.

Lewin, J., & Ashworth, P. J. (2014). The negative relief of large river floodplains. *Earth-Science Reviews*, *129*, 1–23. https://doi.org/10.1016/j.earscirev.2013.10.014

Lewin, J., Ashworth, P. J., & Strick, R. J. P. (2017). Spillage sedimentation on large river floodplains. *Earth Surface Processes and Landforms*, *42*(2), 290–305. https://doi.org/10.1002/esp.3996

Limaye, A. B. (2017). Extraction of multithread channel networks with a reduced-complexity flow model. *Journal of Geophysical Research: Earth Surface*, *122*(10), 1972–1990. https://doi.org/10.1002/2016JF004175

Marriott, S. (1992). Textural analysis and modelling of a flood deposit: River Severn, U.K. *Earth Surface Processes and Landforms*, *17*(7), 687–697. https://doi.org/10.1002/esp.3290170705

McKean, J., & Tonina, D. (2013). Bed stability in unconfined gravel bed mountain streams: With implications for salmon spawning viability in future climates. *Journal of Geophysical Research: Earth Surface*, *118*, 1227–1240. https://doi.org/10.1002/jgrf.20092

Mertes, L. A. K., Dunne, T., & Martinelli, L. A. (1996). Channel-floodplain geomorphology along the Solimões-Amazon River, Brazil. *Bulletin of the Geological Society of America*, *108*(9), 1089–1107. https://doi.org/10.1130/0016-7606(1996)108<1089:CFGATS>2.3.CO;2

Middelkoop, H., Van der perk, M., & Perk, D. (1998). Modelling spatial patterns of overbank sedimentation on embanked floodplains. *Geografiska Annaler—Series A: Physical Geography*, *80*(2), 95–109. https://doi.org/10.1111/j.0435-3676.1998.00029.x

Moody, J. A., Pizzuto, J. E., & Meade, R. H. (1999). Ontogeny of a flood plain. *The Geological Society of America Bulletin*, *111*(2), 291–303. https://doi.org/10.1130/0016-7606(1999)111<0291:ooafp>2.3.co;2

Nanson, G. C. (1980). Point bar and floodplain formation of the meandering Beatton River, northeastern British Columbia, Canada. *Sedimentology*, *27*(1), 3–29. https://doi.org/10.1111/j.1365-3091.1980.tb01155.x

Nanson, G. C. (1986). Episodes of vertical accretion and catastrophic stripping: A model of disequilibrium flood-plain development. *The Geological Society of America Bulletin*, *97*(12), 1467–1475. https://doi.org/10.1130/0016-7606(1986)97<1467:eovaac>2.0.co;2

Nanson, G. C., & Croke, J. C. (1992). A genetic classification of floodplains. *Geomorphology*, *4*, 459–486. https://doi.org/10.1016/0169-555X(92)90039-Q

Nelson, P. A., Venditti, J. G., Dietrich, W. E., Kirchner, J. W., Ikeda, H., Iseya, F., & Sklar, L. S. (2009). Response of bed surface patchiness to reductions in sediment supply. *Journal of Geophysical Research*, *114*(2), 1–18. https://doi.org/10.1029/2008JF001144

Nicholas, A. P., & McLelland, S. J. (2004). Computational fluid dynamics modelling of three-dimensional processes on natural river floodplains. *Journal of Hydraulic Research*, *42*(2), 131–143. https://doi.org/10.1080/00221686.2004.9628299

Nicholas, A. P., & Mitchell, C. A. (2003). Numerical simulation of overbank processes in topographically complex floodplain environments. *Hydrological Processes*, *17*(4), 727–746. https://doi.org/10.1002/hyp.1162

Nicholas, A. P., & Walling, D. E. (1996). The significance of particle aggregation in the overbank deposition of suspended sediment on river floodplains. *Journal of Hydrology*, *186*(1–4), 275–293. https://doi.org/10.1016/S0022-1694(96)03023-5

Nicholas, A. P., & Walling, D. E. (1997). Modelling flood hydraulics and overbank deposition on river floodplains. *Earth Surface Processes and Landforms*, *22*(1), 59–77. https://doi.org/10.1002/(SICI)1096-9837(199701)22:1<59::AID-ESP652>3.0.CO;2-R

Nicholas, A. P., & Walling, D. E. (1998). Numerical modelling of floodplain hydraulics and suspended sediment transport and deposition. *Hydrological Processes*, *12*(8), 1339–1355. https://doi.org/10.1002/(SICI)1099-1085(19980630)12:8<1339::AID-HYP618>3.0.CO;2-6

Nicholas, A. P., Walling, D. E., Sweet, R. J., & Fang, X. (2006). Development and evaluation of a new catchment-scale model of floodplain sedimentation. *Water Resources Research*, *42*(10), 1–13. https://doi.org/10.1029/2005WR004579

Niño, Y. (1995). Particle motion in the near bed region of a turbulent open channel flow: Implications for bedload transport by saltation and sediment entrainment into suspension (doctoral dissertation). *University of Illinois at Urbana-Champaign*.

Niño, Y., & García, M. (1998). Engelund's analysis of turbulent energy and suspended load. *Journal of Engineering Mechanics*, *124*(4), 480–483. https://doi.org/10.1061/(ASCE)0733-9399(1998)124:4(480)

Niño, Y., Lopez, F., & Garcia, M. (2003). Threshold for particle entrainment into suspension. *Sedimentology*, *50*(2), 247–263. https://doi.org/10.1046/j.1365-3091.2003.00551.x

Nolan, K. M., & Marron, D. C. (1995). History, causes, and significance of changes in the channel geometry of Redwood Creek, northwestern California, 1936 to 1982. *Geomorphic Processes and Aquatic Habitat in the Redwood Creek Basin*, Northwestern California (Vol. 1454, pp. N1–N22). US Geological Survey Professional Paper.

Nunnally, N. R. (1967). Definition and identification of channel and overbank deposits and their respective roles in flood plain formation. *The Professional Geographer*, *19*(1), 1–4. https://doi.org/10.1111/j.0033-0124.1967.00001.x

O'Brien, P. E., & Wells, A. T. (1986). A small, alluvial crevasse splay. *Journal of Sedimentary Research*, *56*(6), 876–879. https://doi.org/10.1306/212F8A71-2B24-11D7-8648000102C1865D

Park, E., & Latrubesse, E. M. (2017). The hydro-geomorphologic complexity of the lower Amazon River floodplain and hydrological connectivity assessed by remote sensing and field control. *Remote Sensing of Environment*, *198*, 321–332. https://doi.org/10.1016/j.rse.2017.06.021

Phillips, J. D. (2011). Universal and local controls of avulsions in southeast Texas Rivers. *Geomorphology*, *130*, 17–28. https://doi.org/10.1016/j.geomorph.2010.10.001

Pizzuto, J. E. (1987). Sediment diffusion during overbank flows. *Sedimentology*, *34*(2), 301–317. https://doi.org/10.1111/j.1365-3091.1987.tb00779.x

Pizzuto, J. E., Moody, J. A., & Meade, R. H. (2008). Anatomy and dynamics of a floodplain, powder river, Montana, U.S.A. *Journal of Sedimentary Research*, *78*(1), 16–28. https://doi.org/10.2110/jsr.2008.005

Rak, G., Kozelj, D., & Steinman, F. (2016). The impact of floodplain land use on flood wave propagation. *Natural Hazards*, *83*(1), 425–443. https://doi.org/10.1007/s11069-016-2322-0

Reinfelds, I., & Nanson, G. (1993). Formation of braided river floodplains, Waimakariri River, New Zealand. *Sedimentology*, *40*(6), 1113–1127. https://doi.org/10.1111/j.1365-3091.1993.tb01382.x

Rice, S. (1994). In M. J. Kirkby (Ed.), Towards a model of changes in bed material texture at the drainage basin scale. *Process models and theoretical geomorphology* (pp. 160–172). New York, NY: John Wiley.

Rijn, L. C. V. (1984). Sediment transport, part II: Suspended load transport. *Journal of Hydraulic Engineering*, *110*(11), 1613–1641. https://doi.org/10.1061/(asce)0733-9429(1984)110:11(1613)

Rudorff, C. M., Melack, J. M., & Bates, P. D. (2014). Flooding dynamics on the lower Amazon floodplain: 2. Seasonal and interannual hydrological variability. *Water Resources Research*, *50*(1), 635–649. https://doi.org/10.1002/2013WR014714

Schuurman, F., Marra, W. A., & Kleinhans, M. G. (2013). Physics-based modeling of large braided sand-bed rivers: Bar pattern formation, dynamics, and sensitivity. *Journal of Geophysical Research: Earth Surface*, *118*(4), 2509–2527. https://doi.org/10.1002/2013JF002896

Sturm, T. (2001). *Open hydraulics channel* (Vol. 493). Davis: Univenity of Caldornia.

Thayer, J. B., & Ashmore, P. (2016). Floodplain morphology, sedimentology, and development processes of a partially alluvial channel. *Geomorphology*, *269*, 160–174. https://doi.org/10.1016/j.geomorph.2016.06.040

Trigg, M. A., Bates, P. D., Wilson, M. D., Schumann, G., & Baugh, C. (2012). Floodplain channel morphology and networks of the middle Amazon River. *Water Resources Research*, *48*(10). https://doi.org/10.1029/2012WR011888

USGS. (2020). Retrieved from https://nwis.waterdata.usgs.gov/in/nwis/qwdata/?site_no=03365500&agency_cd=USGS

Van Dijk, W. M., Van de Lageweg, W. I., & Kleinhans, M. G. (2013). Formation of a cohesive floodplain in a dynamic experimental meandering river. *Earth Surface Processes and Landforms*, *38*(13). https://doi.org/10.1002/esp.3400

Viparelli, E., Wesley Lauer, J., Belmont, P., & Parker, G. (2013). A numerical model to develop long-term sediment budgets using isotopic sediment fingerprints. *Computers & Geosciences*, *53*, 114–122. https://doi.org/10.1016/j.cageo.2011.10.003

Wolman, M. G., & Leopold, L. B. (1957). River flood plains: Some observations on their formation. In *U.S. Geological Survey Professional Paper* (pp. 87–109). Reston, VA: U.S. Geological Survey. https://doi.org/10.3133/pp282c

Wolman, M. G., & Miller, J. P. (1960). Magnitude and frequency of forces in geomorphic processes. *The Journal of Geology*, *68*(1), 54–74. https://doi.org/10.1086/626637

Xu, H., Steeg, S., Sullivan, J., Shelley, D., Cely, J. E., Viparelli, E., et al. (2020). Intermittent channel systems of a low-relief, low-gradient floodplain: Comparison of automatic extraction methods. *Water Resources Research*, *56*. https://doi.org/10.1029/2020WR027603

Zwoliński, Z. (1992). Sedimentology and geomorphology of overbank flows on meandering river floodplains. *Geomorphology*, *4*(6), 367–379. https://doi.org/10.1016/0169-555X(92)90032-J